JOURNAL OF THERMOPHYSICS AND HEAT TRANSFER
Vol. 24, No. 3, July–September 2010

Turbulence Modeling Applied to Flow Through a Staggered Tube Bundle

You Qin Wang* and Peter L. Jackson†
University of Northern British Columbia, Prince George, British Columbia V2N 4Z9, Canada

DOI: 10.2514/1.44356

Both two-dimensional and three-dimensional numerical simulations of the turbulent flow through a staggered tube bundle are presented. The primary aim of the present study is to search for a turbulent model that could serve as an engineering design tool at a relatively low computational cost. In the present study, the performances of the Spalart–Allmaras model, the k-ε model, and large eddy simulation are evaluated by comparing their simulation results against experimental measurements. The turbulence models are assessed mainly based on their ability to resolve time-dependent features of the flow related to vortex shedding. Simulations are performed at a Reynolds number of 9300. Overall, the predicted streamwise mean velocity and transverse mean velocity in the present study are in good agreement with measurements, and the results show that the simple one-equation Spalart–Allmaras model could be a very promising tool for numerical simulation of complex turbulent flows, since the Strouhal number obtained by it agrees well with measurements available in the literature for similar tube geometries.

Nomenclature

C_d	=	streamwise drag coefficient, $2F_d/\rho U_\infty^2 \pi d L_z$
d	=	tube diameter, m
F_d	=	streamwise drag force, N
k	=	turbulent kinetic energy, m^2/s^3
L_z	=	computational domain in the z direction, m
Re	=	Reynolds number, $\rho U_\infty d/\mu$
S_L	=	longitudinal pitch, m
S_T	=	transverse pitch, m
T	=	temperature, K
t	=	physical time step, s
t^*	=	nondimensional time step, tU_∞/d
U	=	x-direction mean velocity component, m/s
U_∞	=	inlet velocity, m/s
$\overline{u_i u_j}$	=	Reynolds stress, $(m/s)^2$
u_*	=	friction velocity, m/s
V	=	y-direction mean velocity component, m/s
W	=	z-direction mean velocity component, m/s
x	=	streamwise coordinate, m
y	=	transverse coordinate, m
z	=	spanwise coordinate, m
Δy	=	distance from wall to the first grid point, m
Δy^+	=	first node's wall unit $(=\Delta y u_*/\nu)$
ε	=	turbulent dissipation, m^2/s^3
μ	=	dynamic viscosity, kg/m/s
μ_t	=	turbulent viscosity, kg/m/s
ν	=	kinematic viscosity, m^2/s
ρ	=	fluid density, kg/m^3
ϕ	=	angle measured clockwise from front edge of the tube, deg
ω	=	specific dissipation rate, s^{-1}

Received 13 March 2009; revision received 12 April 2010; accepted for publication 18 April 2010.

*Senior Laboratory Instructor, High Performance Computing Laboratory, College of Science and Management.

†Professor, Environmental Science Program, College of Science and Management.

Introduction

FLOW and heat transfer in tube bundles have many important industrial applications and have been studied in the past both experimentally and through numerical simulation. Many investigations, mostly for steady flow, have been reviewed in two earlier papers [1,2], regarding staggered tube banks and in-line tube banks, respectively. A literature search on unsteady flow associated with vortex shedding in tube bundles reveals that much work has been done in the past on this aspect, especially within the last decade. The experimental results of Abd-Rabbo and Weaver [3] showed that alternate vortex shedding occurs at low Reynolds numbers in staggered arrays. This has been confirmed recently by many flow visualization studies, including Weaver et al. [4] and Price et al. [5]. Recently, Wang et al. [6] have found that alternate vortex shedding also exists at a very high Reynolds number (10^6) in a staggered tube bundle. In experimental studies conducted by Paul et al. [7], the existence of the spatially periodic region was found for all three Reynolds numbers (4800, 9300, and 14,400). Their experimental results indicate that flow evolves fairly rapidly in the streamwise direction and becomes spatially periodic after a relatively short distance. However, because of the complicated flow characteristics in the tube bundles, the vortex structures could not be clearly obtained by their experiment and information on vortex shedding was not reported in their paper [7]. Paul et al. [8] also conducted a two-dimensional numerical investigation of turbulent crossflow over the tube bundle with four Reynolds-averaged Navier–Stokes (RANS) models at a Reynolds number of 9300. They arrived at the conclusion that two-dimensional computations with RANS models for turbulent crossflow over the bundle are not adequate for predicting the mean flow features accurately. It has been noted that the steady models were chosen in their simulations. Therefore, no vortex-shedding information was provided in that paper either. A similar conclusion was obtained by another two-dimensional numerical investigation conducted by Kulasekharan and Prasad [9]. It has been known that for simulation of a developing flow, both upstream and downstream lengths should be long enough so their location will not have a significant impact on the solutions obtained. However, in Kulasekharan and Prasad's study, there are almost no upstream and downstream lengths. In their numerical study, instead of using the periodic boundary condition, a uniform approach velocity was applied to the inlet boundary condition, and the pressure outlet was applied to the outlet boundary condition. With such boundary condition setup, it is thus no surprise that in their study, none of solutions obtained from nine turbulence models were in good agreement with the measurements of Simonin and Barcouda [10]. Recently, large eddy simulation (LES) has become a very popular

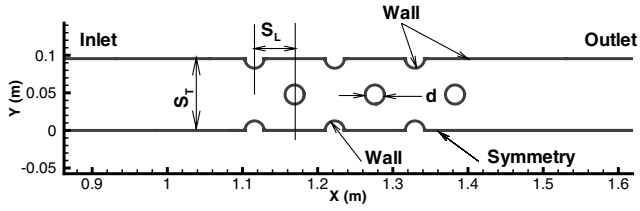

a) Simulation domain with the definition of geometrical parameters

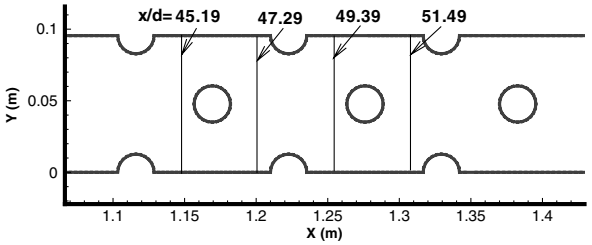

b) Locations at which results are presented

Fig. 1 Two-dimensional simulation domain with the coordinate system.

and reliable numerical method, and has been successfully used in prediction of flow around tube bundles, such as in simulations conducted by Barsamian and Hassan [11], Bouris and Bergeles [12], Mollet-Miet et al. [13], and Benhamadouche and Laurence [14]. However, most of the numerical simulations of the turbulent flow around tube bundles that have been performed to date are based on one (or more) of the following simplifying assumptions: low Reynolds number laminar flow, statistically steady turbulent flow, or fully developed periodic flow in the streamwise and cross-stream direction. It should be noted that in an numerical investigation conducted by Liang and Papadakis [15], the aforementioned limitations were removed. They studied the flow development in a staggered array consisting of six rows at a Reynolds number of 8600 by three-dimensional LES. Two distinct vortex-shedding frequencies were reported behind the first two rows, but the high-frequency component vanished in the downstream rows. The corresponding Strouhal numbers agree well with those of experimental findings.

Table 1 Grid information: coarse grid (*G*1-*O*), coarse grid with refinement (*G*1-*A*), finer grid (*G*2-*O*), and finer grid with refinement (*G*2-*A*)

	S-A model		k-ε model	
Mesh	Cells	Δy^+	Cells	Δy^+
*G*1-*O*	50,482	3.71	50,482	3.84
*G*1-*A*	83,605	1.04	75,412	1.03
*G*2-*O*	111,580	4.53	111,580	3.86
*G*2-*A*	133,924	1.12	132,607	1.01

The primary aim of the present study is to search for a turbulent model that could serve as an engineering design tool at a relatively low computational cost. The performances of the Spalart–Allmaras model (referred to as the S-A model throughout), the k-ε model, and LES are evaluated by comparing their simulation results against experimental measurements. The turbulence models are assessed mainly based on their ability to resolve time-dependent features of the flow related to vortex shedding.

The rest of the paper is arranged as follows. First, the geometry and computational grids are presented, followed by the numerical approach and turbulence models. The predicted streamwise mean velocity and transverse mean velocity are then validated against detailed experimental data. Following validation, instantaneous flow patterns are analyzed and the temporal evolution of vorticity are presented. Finally, the associated Strouhal numbers are compared with available experimental results.

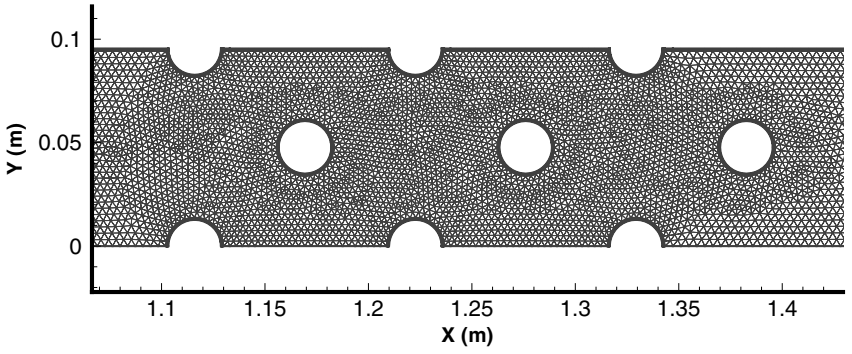

a) Coarse grid at tube bank

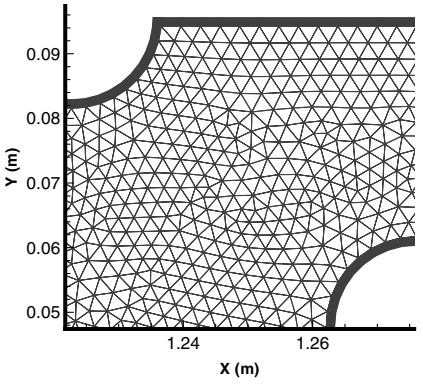

b) Coarse grid detail

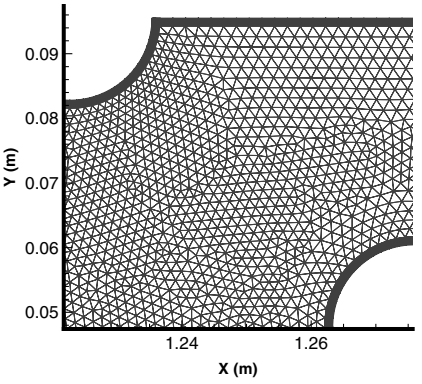

c) Fine grid detail

Fig. 2 Sample grid detail.

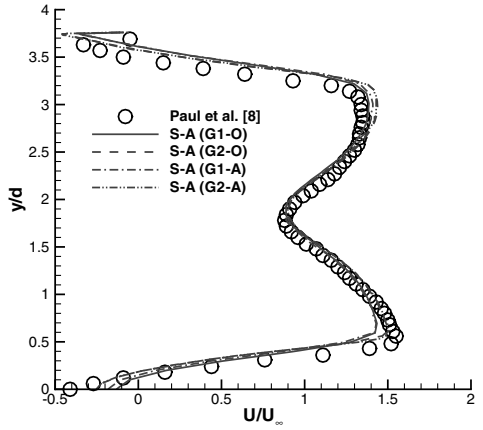

a) Streamwise mean velocity by S-A model

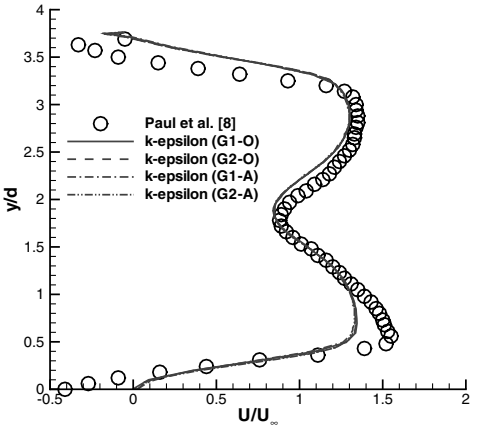

b) Streamwise mean velocity by k-ε model

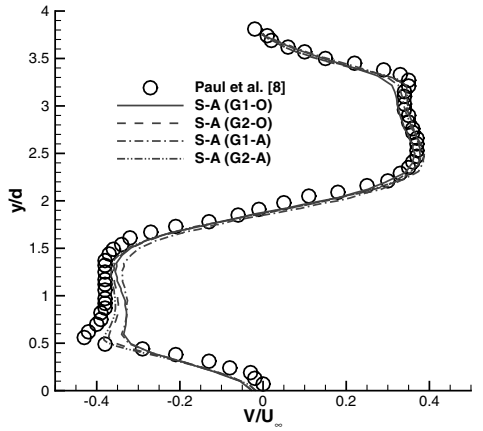

c) Transverse mean velocity by S-A mode

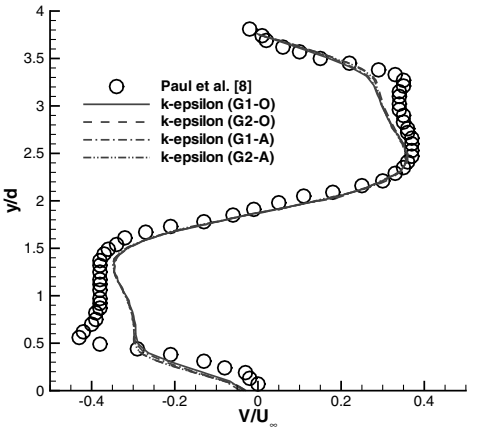

d) Transverse mean velocity by k-ε model

Fig. 3 Sample profiles of the grid-independence test of streamwise mean velocity and transverse mean velocity at $x/d = 45.19$.

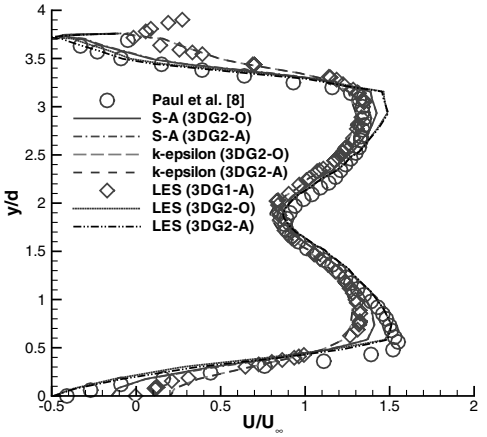

a) Streamwise mean velocity

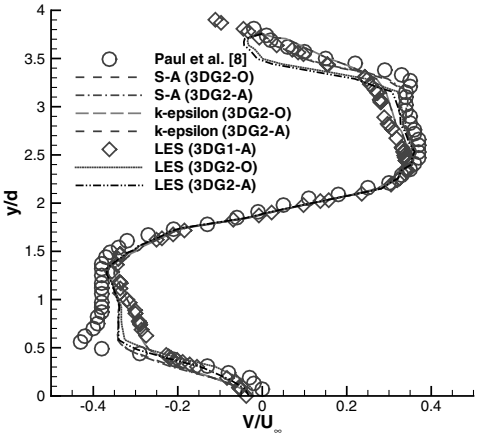

b) Transverse mean velocity

Fig. 4 Sample profiles of the grid-independence test of the streamwise mean velocity and transverse mean velocity at $x/d = 11.25$.

Simulation Overview

Problem Description

The geometry of the two-dimensional domain representing a typical region in a bundle with tube diameter $d = 0.0254$ m, transverse pitch $S_T = 0.0955$ m, and longitudinal pitch $S_L = 0.05334$ m is shown in Fig. 1a. Figure 1b shows the details of the region, in which most results will be presented using spatial coordinates normalized by the tube diameter. The case was originally studied by

Table 2 Grid information: coarse grid (*G1-O*), coarse grid with refinement (*G1-A*), finer grid (*G2-O*), and finer grid with refinement (*G2-A*)

	LES		S-A model		k-ε model	
Mesh	Cells	Δy^+	Cells	Δy^+	Cells	Δy^+
3D*G2-O*	824,064	5.87	824,064	3.89	824,064	3.99
3D*G2-A*	1,067,286	4.81	1,335,330	2.82	1,008,843	2.36

Paul et al. [7] using particle image velocimetry. In two-dimensional study, the simulation domain is 2.5×0.0955 m, which is half of the experimental domain in the transverse direction because a combination of symmetry and no-slip boundary condition is applied at the bottom edge. For two-dimensional simulations, the distance from the inlet to the center of the first tube and the distance from the center of the last tube to the outlet are taken to be $43.9d$ and $44.0d$ respectively, which are identical to the Paul et al. [7] experimental setup. For three-dimensional simulations, due to the higher computational cost, the distance from the inlet to the center of the first tube and the distance from the center of the last tube to the outlet are taken to be $10d$ and $15d$, respectively. These lengths were judged to be sufficiently long so that any increase in their values would not have a significant impact on the solutions obtained. In two-dimensional simulations conducted by Paul et al. [8], the upstream and downstream lengths are both taken to be only $10d$.

Grid and Numerical Approach

Two-Dimensional Grid

Two mesh schemes are generated for the calculations and the grid-sensitivity study. The examples of coarse grid are presented in Figs. 2a and 2b, and the example of finer grid is presented in Fig. 2c. The coarse grid (referred to as *G*1-*O* throughout) consists of 50,482 cells with a maximum volume of 1.02×10^{-5} m^3, and the finer grid (referred to as *G*2-*O* throughout) consists of 111,580 cells with a maximum volume of 4.57×10^{-6} m^3. Both mesh schemes were generated having a thin boundary layer around all tubes and the top wall. Irregular triangular mesh elements were used for both schemes. The important advantage of using irregular triangular mesh elements is that the mesh aligned to the tube corners on top and bottom boundaries does not need to be stretched as the structured mesh does. It was found that mesh *G*2-*O* has a higher quality regarding the mesh skewness. Both solution-adaptive refinement and boundary-adaptive refinement (features of FLUENT) were used in the calculation domain, mainly in the tube bank region. Gradients of velocity magnitude and turbulent quantities have been selected as the field variables for adapting the grid. The number of grid points after refinement for calculations with two different models is given in Table 1. After refinement, all Δy^+ values are less than 2 in the flow domain for the simulations, and the finest grid consists of 133,924 cells.

Figure 3 shows the streamwise mean velocity and transverse mean velocity at $x/d = 45.19$ as predicted on different grids by the S-A model and the k-ε model. It is observed that mean velocity profiles obtained by the k-ε model on four grid sets are practically identical. Simulation results obtained by the S-A model were more sensitive to grid refinement. The profiles of transverse mean velocity obtained with fine grids were closer to the experimental data than the profiles of transverse mean velocity obtained with coarse grids. However, the differences among solutions obtained by two fine grid sets (*G*2-*O* and *G*2-*A*) are difficult to detect. In the rest of this paper, only results from *G*2-*O* are presented, unless otherwise stated.

Three-Dimensional Grid

In three-dimensional study, one simulation domain is set to be $0.9017 \times 0.0955 \times 0.0762$ m with 824,064 cells (3D*G*2-*O*). Another grid scheme is generated for grid-independence study purpose and only LES is performed on it. That simulation domain is set to be $2.5 \times 0.191 \times 0.2$ m with 1,732,895 cells (3D*G*1-*O*). After refinement, the cells number reaches 2,021,414. The simulation

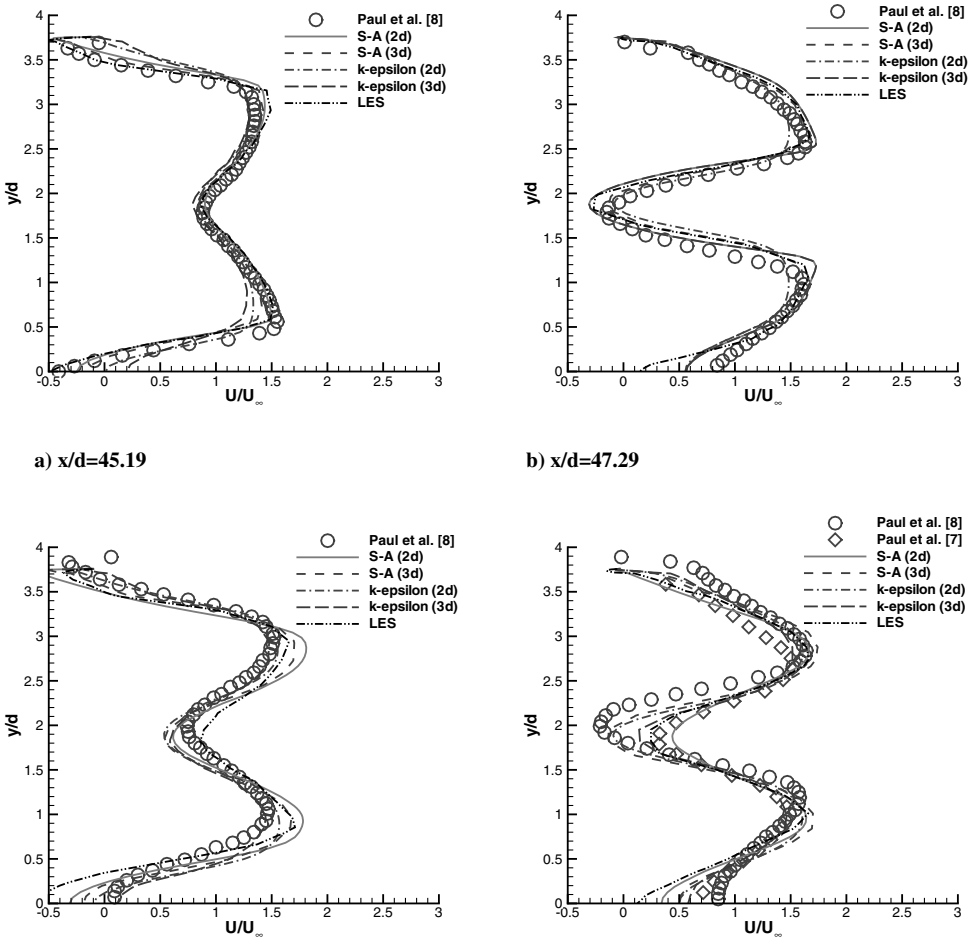

Fig. 5 Comparison of streamwise mean velocity at selected axial locations (see Fig. 1b).

results plotted in Fig. 4 indicate that the agreement between the solutions obtained by LES on two grids is reasonably good although the grid 3D*G*1-*A* is very coarse. Figure 4 also indicates that both streamwise mean velocity and transverse mean velocity predicted by S-A model, k-ε model, and LES were not sensitive to the grid refinement. In the rest of this paper, only results from the finer grid with the refinement (3D*G*2-*A*) are presented. The grid refinement information for three models is summarized in Table 2. It should be noted that even after refinement, the grids are still relatively coarse compared to those used in the two-dimensional simulations.

Numerical Approach

The boundary conditions for the solution domain shown in Fig. 1a are as follows. Fluid with an approach velocity U_∞ enters the solution domain uniformly at the inlet region, and a combination of symmetry and no-slip boundary condition is used at the bottom edge. In addition, at the inlet the turbulent intensity, based on the experimental data, is set equal to 4%. A pressure-outlet boundary condition was used to define the static pressure at the flow outlet, and it was set to be equal to the operating pressure of 101,325 Pa (default value in FLUENT [16]). For all the calculations, a segregated solution approach using the SIMPLE algorithm was used. The governing equations were discretized by the second-order upwind scheme. A second-order implicit scheme was used for the unsteady formulation. The nondimensional time step ($t^* = tU_\infty/d$) for calculations was 0.015. The simulations were performed on an SGI Altix 3000 with up to eight CPUs.

For the S-A model, it took approximately 13 and 136 s on *G*2-*A* and 3D*G*2-*A*, respectively, to complete one time step. Each time step took around 11 subiterations to converge for the two-dimensional case and around five subiterations to converge for the three-dimensional case. For the k-ε model, it took approximately 10 and 73 s on *G*2-*A* and 3D*G*2-*A*, respectively, to complete one time step. Each time step took about four subiterations to converge for both two-dimensional and three-dimensional simulations. For LES, it took approximately 504 s on 3D*G*2-*A* to complete one time step, and each time step took around 18 subiterations to converge. On 3D*G*1-*A*, it took approximately 792 s to complete one time step and each time step took about eight subiterations to converge. At least 6000 time steps were used to obtain the time-averaged results, and convergence was declared when the maximum scaled residuals were less than 10^{-4} for all governing equations.

Turbulence Models

Three turbulence models are investigated in the present study: the S-A model, the k-ε model, and LES. The S-A model is a relatively simple one-equation model that solves a modeled transport equation for the kinematic eddy viscosity [17], while in LES, large eddies are resolved directly and small eddies are modeled. The details of their mathematical formulation and their implementation in FLUENT can be found in the authors' previous publication [18] and are not presented in this paper, due to space limitations. The standard k-ε model is a semi-empirical, two-equation model based on model transport equations for the turbulence kinetic energy k and its

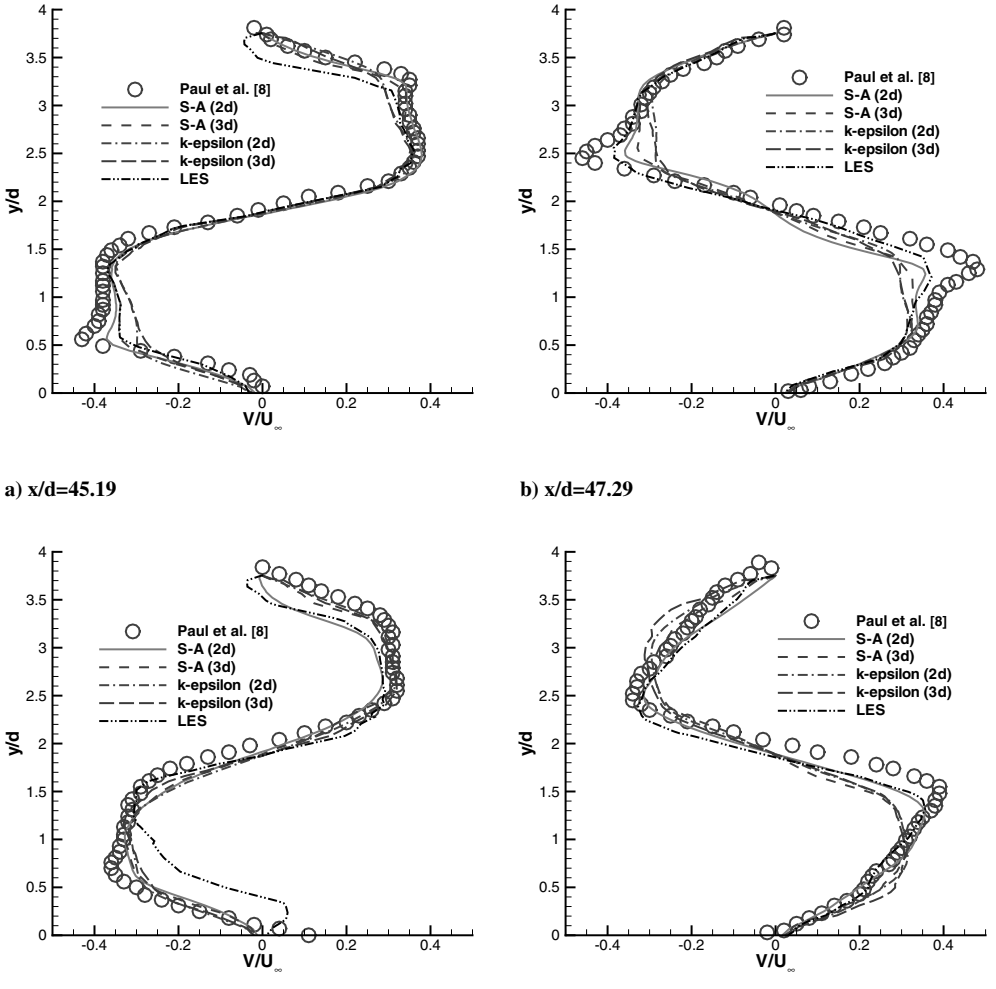

a) x/d=45.19 **b) x/d=47.29**

c) x/d=49.39 **d) x/d=51.49**

Fig. 6 Comparison of transverse mean velocity at selected axial locations (see Fig. 1b).

dissipation rate ε originally proposed by Launder and Spalding [19]. The model transport equation for k is derived from the exact equation, while the model transport equation for ε was obtained using physical reasoning and is not mathematically exact.

The turbulence kinetic energy k and its rate of dissipation ε are obtained from the following transport equations:

$$\frac{\partial}{\partial t}(\rho k) + \frac{\partial}{\partial x_i}(\rho k u_i) = \frac{\partial}{\partial x_j}\left[\left(\mu + \frac{\mu_t}{\sigma_k}\right)\frac{\partial k}{\partial x_j}\right] + G_k + G_b - \rho\varepsilon \tag{1}$$

and

$$\frac{\partial}{\partial t}(\rho\varepsilon) + \frac{\partial}{\partial x_i}(\rho\varepsilon u_i) = \frac{\partial}{\partial x_j}\left[\left(\mu + \frac{\mu_t}{\sigma_\varepsilon}\right)\frac{\partial \varepsilon}{\partial x_j}\right] + C_{1\varepsilon}\frac{\varepsilon}{k}(G_k + C_{3\varepsilon}) - C_{2\varepsilon}\rho\frac{\varepsilon^2}{k} \tag{2}$$

In these equations, G_k represents the generation of turbulence kinetic energy due to the mean velocity gradients, calculated as

$$G_k = -\rho\overline{u_i' u_j'}\frac{\partial u_j}{\partial x_i} \tag{3}$$

The turbulent (or eddy) viscosity μ_t is computed by combining k and ε as follows:

$$\mu_t = \rho C_\mu \frac{k^2}{\varepsilon} \tag{4}$$

The model constants $C_{1\varepsilon}$, $C_{2\varepsilon}$, C_μ, σ_k, and σ_ε have the following default values:

$$C_{1\varepsilon} = 1.44, \quad C_{2\varepsilon} = 1.92, \quad C_\mu = 0.09, \quad \sigma_k = 1.0, \quad \sigma_\varepsilon = 1.3$$

Results and Discussion

Mean Velocity Profiles and RMS Velocities

The distribution of the dimensionless streamwise and transverse mean velocities obtained with two-dimensional and three-dimensional grids at selected x/d locations are shown together with the experimental measurements in Figs. 5 and 6. The experimental data are extracted from Figs. 9 and 10 in Paul et al. [8]. Figures 5 and 6 reveal that all models produce the correct trends of the streamwise and transverse mean velocity profiles at all x/d locations. In Fig. 5, in the flow-developing region ($x/d \leq 47.29$), the streamwise mean velocity obtained in the present study is in very good agreement with the measurements (see Figs. 5a and 5b), while a relatively larger disagreement between the simulation and the measurements occurs in the spatially periodic region ($x/d > 47.29$, see Figs. 5c and 5d). However, in all four locations, the present simulations appear to be in better agreement with the measurements than the numerical simulation results conducted by Paul et al. [8]. In their numerical study, four turbulence models were used and none of them were able to consistently reproduce the mean velocity well. It should be noted that in Fig. 5d, experimental data are extracted from Fig. 4 in [7] and Fig. 9 in [8] because it has been found that at the same location, the difference between the experimental data reported in two papers is obvious. In Fig. 6b, results from the S-A model and LES are in better agreement with the experimental data than results

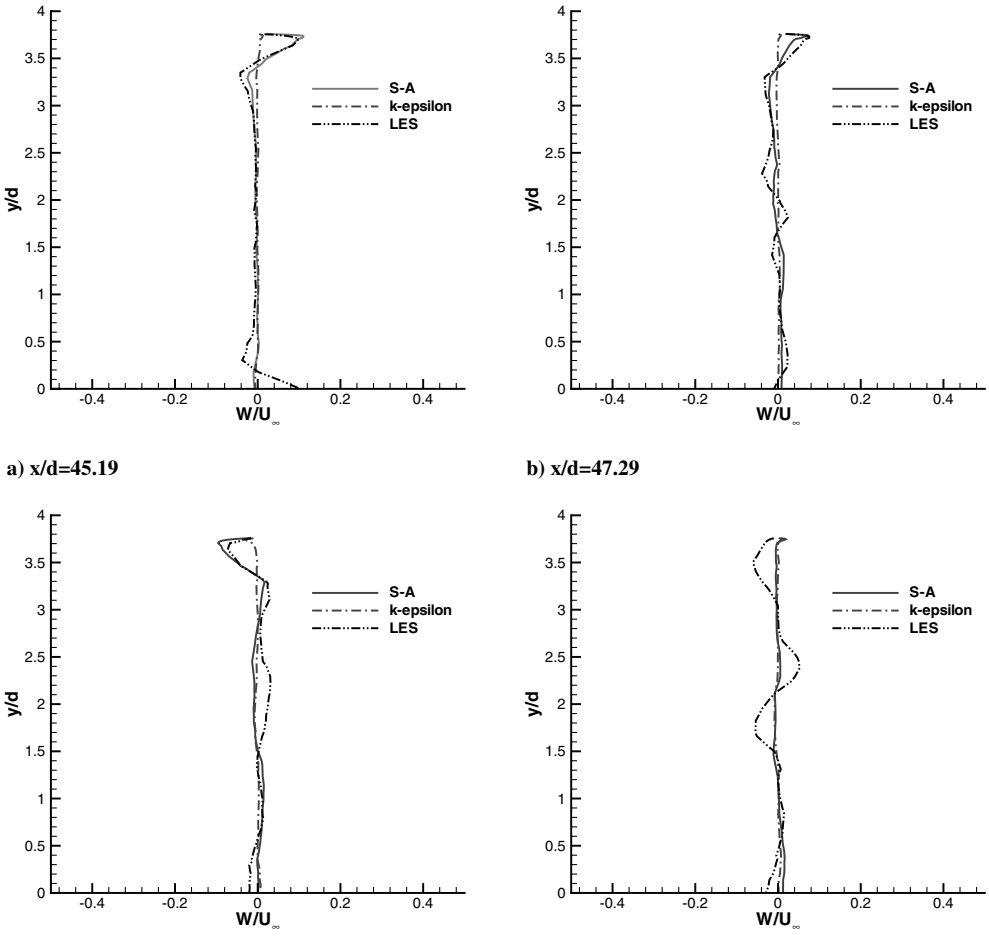

Fig. 7 Comparison of spanwise mean velocity at selected axial locations at $z/d = 1.5$ (see Fig. 1b).

from the k-ε model. The predicted transverse mean velocities obtained by k-ε model have underpredicted the peak values. This behavior is consistent with the model performance in the previous numerical study [8]. At $x/d = 49.39$, the present simulations obtained using the k-ε model and three-dimensional S-A model appear to be in much better agreement with the measurements than solutions obtained with two-dimensional S-A and LES. At $x/d = 51.49$, the results obtained by two-dimensional S-A and LES appear to be in much better agreement with the measurements than solutions obtained with k-ε model. The distribution of the dimensionless spanwise mean velocities obtained with three-dimensional grids at selected x/d locations are shown in Fig. 7. The spanwise mean velocity is much smaller compared with streamwise mean velocity and transverse mean velocity plotted in Figs. 5 and 6, indicating that the mean flow structure is dominated by only streamwise mean velocity and transverse mean velocity. Unfortunately, there are no spanwise mean velocities obtained from previous studies available for comparison. Overall, in the present study, mean velocity profiles obtained by all models are in good agreement with the experimental data. Most likely because the three-dimensional grid was too coarse, no three-dimensional solutions appear superior to two-dimensional solutions, and LES has no advantage over the S-A model or k-ε model.

RMS velocities from the simulations are examined and compared with Paul et al. [7]. The simulated RMS velocities did not compare as well with previous observations as did the mean velocities. Specifically, it has been found that the largest RMS values developed after the fourth tube row in the S-A simulations, rather than after the second tube row, as previous observations would suggest. The RMS values from the k-ε were delayed even further, not developing until after the sixth tube row. The LES had a similar difficulty in simulation of RMS values.

Instantaneous Streamlines, Vorticity Contours, and Temperature Contours

Some previous studies have clearly shown that alternate vortex shedding occurs at discrete frequencies inside tube arrays over a wide range of configurations and Reynolds numbers. Closer examination of the instantaneous flow patterns in tube bundle reveals that in the present study, only the S-A model and LES are capable of capturing the spatially periodic flow structure. The streamlines of the instantaneous flow over tubes obtained by the three models are shown in Fig. 8. Figure 8a reveals that the flow is nearly symmetrical around the forward portion of the tube. The stagnation point (point B) is located at the middle-tube horizontal centerline. The separations occur at an angle of $\phi = 102$ and 258° on the top part of the tube and on the bottom part of the tube, respectively. Two unsymmetrical vortices are observed downstream from the tube that indicate that flow has a spatially periodic structure after the second tube row. This finding is consistent with that of Paul et al. [7]. It was found from their experimental study that the flow develops very rapidly through the tube bundle and becomes spatially periodic after the second tube row. In Fig. 8b, unlike in Fig. 8a, the stagnation point at the fourth tube row has been shifted away from the middle-tube horizontal centerline. The separations occur at an angle of $\phi = 102°$ on the top part of the tube and at an angle of $\phi = 234°$ on the bottom part of the tube. Two vortices, different in size and opposite in rotational direction, are formed downstream of the tube. The size of the recirculation region is much smaller than that behind the tube in the second row. From the streamlines around the sixth tube row, it can be seen that the

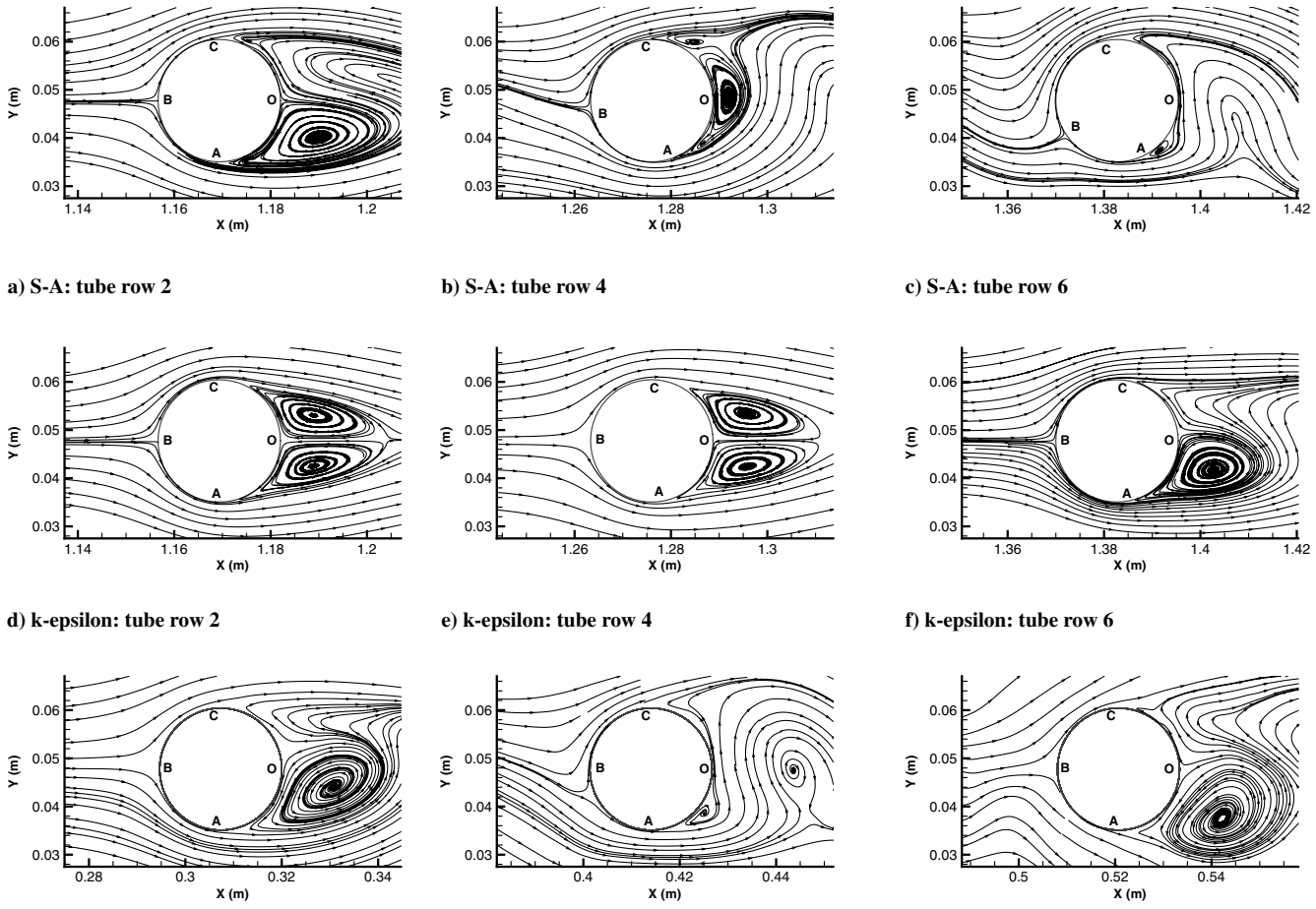

a) S-A: tube row 2 b) S-A: tube row 4 c) S-A: tube row 6

d) k-epsilon: tube row 2 e) k-epsilon: tube row 4 f) k-epsilon: tube row 6

g) LES: tube row 2 h) LES: tube row 4 i) LES: tube row 6

Fig. 8 Instantaneous flowfield around tubes.

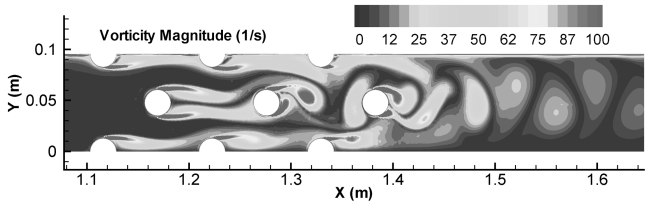

a) $t = 14.00\,(s)$

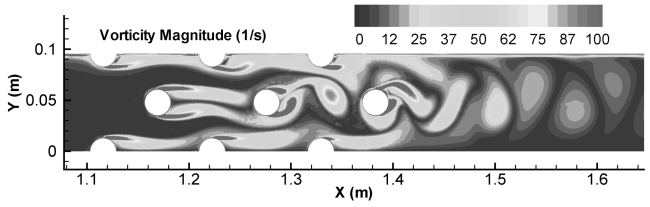

b) $t = 14.05\,(s)$

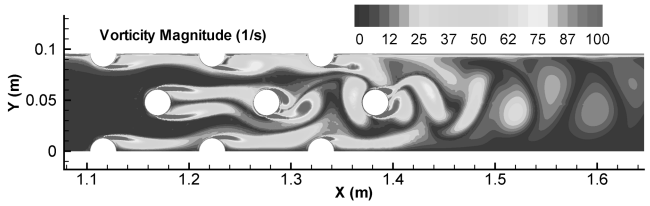

c) $t = 14.10\,(s)$

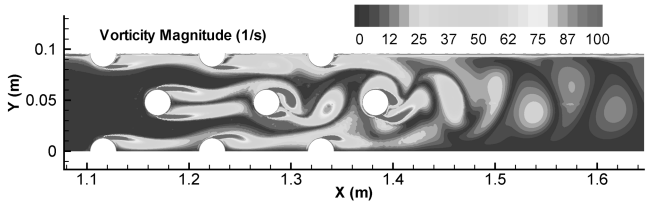

d) $t = 14.15\,(s)$

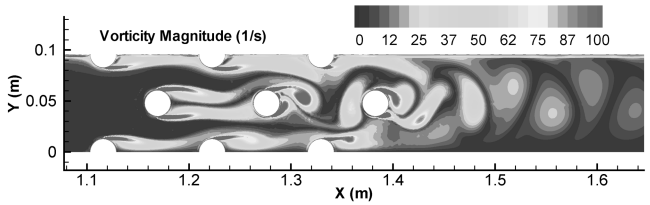

e) $t = 14.20\,(s)$

Fig. 9 Temporal evolution of vorticity obtained by the S-A model.

stagnation point was pushed down further compared with that of the fourth tube row. The separations occur at an angle of $\phi = 108°$ on the top part of the tube and at an angle of $\phi = 246°$ on the bottom part of the tube (see Fig. 8c). The streamlines of the instantaneous flow over tubes obtained by the k-ε model are shown in Figs. 8d–8f. Two vortices, similar in size but opposite in rotational direction, are formed downstream of both tubes in row two and row four. Around the sixth tube row, flow is still near symmetrical in the forward portion of the tube. The solution obtained by the k-ε model indicates that flow becomes spatially periodic after the sixth tube row. The flow develops much slower through the tube bundle in comparison with the experiments. The streamlines of the instantaneous flow over tubes at $z/d = 1.5$ obtained by LES are shown in Figs. 8g–8i. Unsymmetrical streamlines are observed downstream from the second tube row, and flow patterns are similar to those observed with the two-dimensional S-A model.

Figure 9 presents the evolution of the vorticity fields around the tubes from $t = 14.00$ to 14.20 s obtained by the two-dimensional S-A model. It clearly captures the character of the vortex shedding. Only the evolution of the vortex around the tube in row four is discussed here. The sequence begins in Fig. 9a with a vortex that has just detached from the upper surface of the tube. A new vortex has already started to form on the lower surface of the tube. When the detached vortex moves downstream and passes the gap between the tubes in row five, it is stretched (Fig. 9b). The vortex continues to move downstream toward the front wall of the tube in row six. Before it hits the front of the tube wall, it can still be distinguished. However, there is no evidence of this vortex surviving past tube row six. While this detached vortex moves downstream, the vortex that is still attached to the lower surface of the tube continues to grow until it is finally shed (Fig. 9c). At the same time, the vortex that has already formed on the upper surface of the tube continues to grow (Fig. 9d). Finally, when this vortex grows too large to remain attached to the tube, it is shed (Fig. 9e). Figure 9e is similar to Fig. 9a, as the flow starts a new vortex-shedding cycle.

Figure 10 presents the instantaneous vorticity field around the tubes obtained by the two-dimensional k-ε model and three-dimensional LES. Unlike the solutions obtained by the S-A model, in Fig. 10a, there is no spatially periodic structure observed through the tube bundle, and the alternate vortex shedding only occurs after the sixth tube row. Downstream from the last tube row in Fig. 10b, a large number of smaller-scale eddies, nonexistent in both the S-A and k-ε calculations, are observed in the vorticity field from the LES.

Because of a very high computational cost involved in three-dimensional simulations, the energy equation was only included in two-dimensional calculations. The instantaneous temperature contours obtained by the S-A model and the k-ε model are presented in Fig. 11. The higher-temperature areas were not only observed in the recirculation regions behind each tube but were also strongly associated with the vortex shedding in the spatially periodic region.

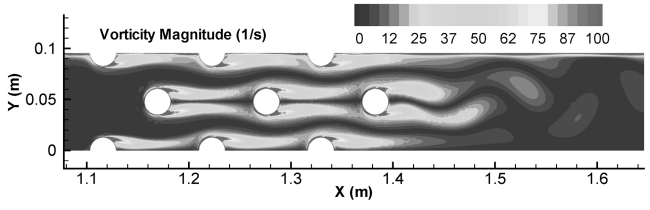

a) k-ε model at t=14.00 (s)

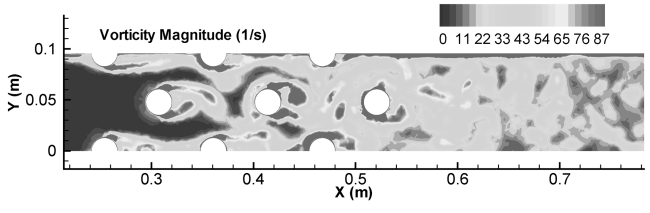

b) LES at t=11.50 (s)

Fig. 10 Instantaneous vorticity contour.

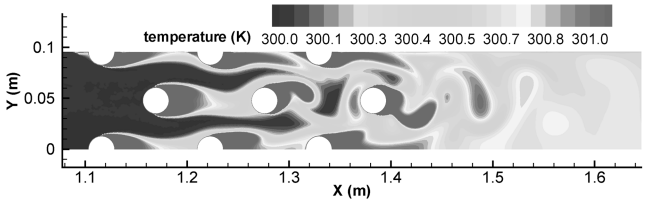

a) S-A model at t=14.00 (s)

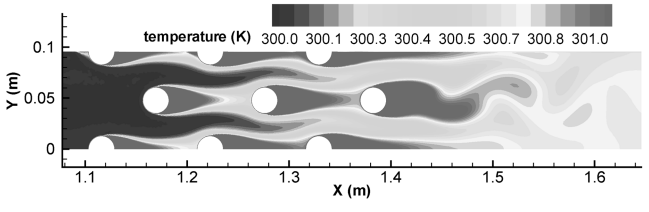

b) k-ε model at t=14.00 (s)

Fig. 11 Instantaneous temperature contour.

This finding is consistent with that of Beale and Spalding [20]. Their numerical results reveal that the formation of the vortices has a significant effect on the temperature field in both in-line and staggered tube bundles at the Reynolds number of 300.

Statistical Features for Unsteady Flow

Part of the temporal evolution of the streamwise drag force coefficient and the frequency spectra of the streamwise drag coefficient are shown in Figs. 12 and 13, respectively. The simulation results shown were taken around the fourth tube row obtained by the two-dimensional S-A model, two-dimensional k-ε model, and the three-dimensional LES. There are important differences in the magnitude and nature of the streamwise drag coefficient in Fig. 12. Streamwise drag coefficient in the k-ε is small and constant, whereas S-A predicts a significant variation around the mean with a regular pattern, consistent with a regular vortex-shedding frequency. Furthermore, LES predicts a more significant variation around the mean with no regular pattern, consistent with the random nature of the shedding and in agreement with observations from experiments with similar tube geometries [21].

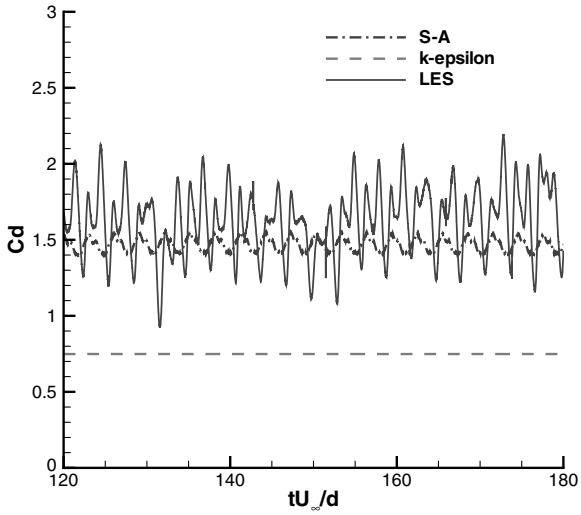

Fig. 12 Temporal evolution of the streamwise drag coefficient around the fourth tube row.

In Fig. 13, the frequency has been converted to a Strouhal number. In S-A, the peak value was 0.345 (or $St = 0.254$ based on the gap velocity), which corresponded to $f = 5.00/\mathrm{s}$, i.e., it took approximately 0.20 s to complete a whole vortex-shedding cycle. The value estimated from flow visualization discussed in Fig. 9 is also 0.20 s, and it perfectly matches with the peak value obtained by statistical analysis. In LES, two Strouhal numbers are detected around the fourth tube row, and the dominant Strouhal number is same as observed in S-A. This dominant Strouhal number was attributed to von Karman vortex shedding, which agrees well with the experimental value of 0.35 (or $St = 0.26$ based on the gap velocity) of Balabani and Yianneskis [21,22]. However, the origin of the second periodicity detected in LES remains uncertain. The experimental value of 0.37 was obtained by Weaver et al. [4] for a rotated square array with a pitch ratio of 2.42. In LES of Liang and Papadakis [15], the dominant Strouhal number, which was detected behind all tube rows, is 0.38. However, they observed that the second Strouhal number, only detected behind the first two rows, had a value of 0.49. This disagreement with the present results may stem from differences in the tube spacing and Reynolds number.

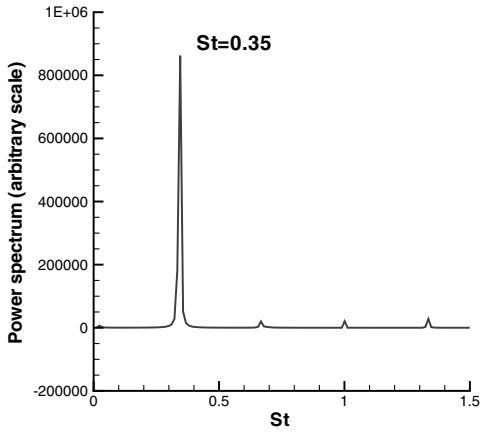

a) SA model

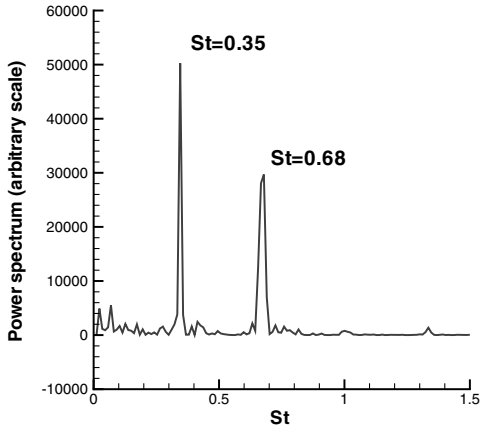

b) LES

Fig. 13 Power spectra of the streamwise drag coefficient.

Conclusions

The S-A model, k-ε model, and LES have been used to simulate the flow through a staggered tube bundle at $Re = 9300$. In two-dimensional simulations, both the S-A model and the k-ε model reproduce better predictions in the mean quantities than the previous two-dimensional numerical studies [8,9]. The comparison of the two-dimensional simulation results with experimental data [7] shows that the solutions obtained using the S-A model successfully predicted the locations where flow becomes spatially periodic but in the solutions obtained using the k-ε model, the flow develops much slower through the tube bundle. Furthermore, the vortex-shedding frequency detected by the two-dimensional S-A is identical with the vortex shedding detected by the three-dimensional LES, which agrees very well with previous published data for similar tube geometries. In the future, the two-dimensional S-A model could become a very promising numerical simulation tool in industrial design, due to its lower computational cost in comparison with other turbulence models. In mean velocity prediction, no three-dimensional solutions appear superior to two-dimensional solutions, and LES has no advantage over the other approaches.

Acknowledgments

Computing infrastructure for this work was provided by grants from the Canada Foundation for Innovation; British Columbia Knowledge Development Fund; Silicon Graphics, Inc., Canada; and donors to the University of Northern British Columbia.

References

[1] Wang, Y. Q., Penner, L. A., and Ormiston, S. J., "Analysis of Laminar Forced Convection of Air for Crossflow in Banks of Staggered Tubes," *Numerical Heat Transfer, Part A, Applications*, Vol. 38, No. 8, 2000, pp. 819–845. doi:10.1080/104077800457449

[2] El-Shaboury, A. M. F., and Ormiston, S. J., "Analysis of Laminar Forced Convection of Air Crossflow in In-Line Tube Banks with Nonsquare Arrangements," *Numerical Heat Transfer, Part A,*

Applications, Vol. 48, No. 2, 2005, pp. 99–126.
doi:10.1080/10407780590945452

[3] Abd-Rabbo, A., and Weaver, D. S., "A Flow Visualization Study of Flow Development in a Staggered Tube Array," *Journal of Sound and Vibration*, Vol. 106, No. 2, 1986, pp. 241–256.
doi:10.1016/0022-460X(86)90316-0

[4] Weaver, D. S., Lian, H. Y., and Huang, X. Y., "Vortex Shedding in Rotated Square Arrays," *Journal of Fluids and Structures*, Vol. 7, No. 2, 1993, pp. 107–121.
doi:10.1006/jfls.1993.1009

[5] Price, S. J., Paidoussis, M. P., and Mark, B., "Flow Visualization of the Interstitial Crossflow Through Parallel Triangular and Rotated Square Arrays of Cylinders," *Journal of Sound and Vibration*, Vol. 181, No. 1, 1995, pp. 85–98.
doi:10.1006/jsvi.1995.0127

[6] Wang, Y. Q., Jackson, P. L., and Phaneuf, T. J., "Turbulent Flow Through a Staggered Tube Bank," *Journal of Thermophysics and Heat Transfer*, Vol. 20, No. 4, 2006, pp. 738–746.
doi:10.2514/1.18973

[7] Paul, S. S., Tachie, M. F., and Ormiston, S. J., "Experimental Study of Turbulent Crossflow in a Staggered Tube Bundle Using Particle Image Velocimetry," *International Journal of Heat and Fluid Flow*, Vol. 28, No. 3, 2007, pp. 441–453.
doi:10.1016/j.ijheatfluidflow.2006.06.001

[8] Paul, S. S., Ormiston, S. J., and Tachie, M. F., "Experimental and Numerical Investigation of Turbulent Crossflow in a Staggered Tube Bundle," *International Journal of Heat and Fluid Flow*, Vol. 29, No. 2, 2007, pp. 387–414.

[9] Kulasekharan, N., and Prasad, B. V. S. S. S., "Performance of 2-D Turbulence RANS Models for Prediction of Flow Past a Staggered Tube Bank Array," *Engineering Applications of Computational Fluid Mechanics*, Vol. 3, No. 3, 2009, pp. 386–407.

[10] Simonin, O., and Barcouda, M., "Measurements and Prediction of Turbulent Flow Entering a Staggered Tube Bundle," *Proceedings of the Fourth International Symposium on Applications of Laser Anemometry to Fluid Mechanics*, Lisbon, 1988.

[11] Barsamian, H. R., and Hassan, Y. A., "Large Eddy Simulation of Turbulent Crossflow in Tube Bundles," *Nuclear Engineering and Design*, Vol. 172, No. 1, 1997, pp. 103–122.
doi:10.1016/S0029-5493(97)00034-4

[12] Bouris, D., and Bergeles, G., "Two Dimensional Time Dependent Simulation of the Subcritical Flow in a Staggered Tube Bundle Using a Subgrid Scale Model," *International Journal of Heat and Fluid Flow*, Vol. 20, No. 2, 1999, pp. 105–114.
doi:10.1016/S0142-727X(98)10053-X

[13] Mollet-Miet, P., Laurence, D., and Ferziger, J., "LES and RANS of Turbulent Flow in Tube Bundles," *International Journal of Heat and Fluid Flow*, Vol. 20, No. 3, 1999, pp. 241–254.
doi:10.1016/S0142-727X(99)00006-5

[14] Benhamadouche, S., and Laurence, D., "LES, Coarse LES, and Transient RANS Comparisons on the Flow Across a Tube Bundle," *International Journal of Heat and Fluid Flow*, Vol. 24, No. 4, 2003, pp. 470–479.
doi:10.1016/S0142-727X(03)00060-2

[15] Liang, C., and Papadakis, G., "Large Eddy Simulation of Crossflow Through a Staggered Tube Bundle at Subcritical Reynolds Number," *Journal of Fluids and Structures*, Vol. 23, No. 8, 2007, pp. 1215–1230.
doi:10.1016/j.jfluidstructs.2007.05.004

[16] *FLUENT 6.3 User's Guide*, Fluent, Inc., Natick, MA, 2006, Chap. 7, Sec. 8.

[17] Spalart, P. R., and Allmars, S. R., "A One-Equation Turbulence Model for Aerodynamic Flows," *La Recherche Aerospatiale : Bulletin Bimestriel de l'Office National d'Etudes et de Recherches Aerospatiales*, Vol. 1, No. 1, 1994, pp. 5–21.

[18] Wang, Y. Q., Jackson, P., and Ackerman, J., "Numerical Investigation of Flow over a Sphere Using LES and the Spalart–Allmaras Turbulent Model," *Computational Fluid Dynamics Journal*, Vol. 15, No. 1, 2006, pp. 198–205.

[19] Launder, B. E., and Spalding, D. B., "Lectures in Mathematical Models of Turbulence," Academic Press, London, 1972.

[20] Beale, S. B., and Spalding, D. B., "A Numerical Study of Unsteady Fluid Flow in In-Line and Staggered Tube Banks," *Journal of Fluids and Structures*, Vol. 13, No. 6, 1999, pp. 723–754.
doi:10.1006/jfls.1999.0231

[21] Balabani, S., and Yianneskis, M., "Vortex Shedding and Turbulence Scales in Staggered Tube Bundle Flows," *Canadian Journal of Chemical Engineering*, Vol. 75, No. 5, 1997, pp. 823–831.
doi:10.1002/cjce.5450750502

[22] Balabani, S., and Yianneskis, M., "An Experimental Study of the Mean Flow and Turbulence Structure of Crossflow over Tube Bundle," *Proceedings of the Institution of Mechanical Engineers Part C, Mechanical Engineering Science*, Vol. 210, No. 43, 1996, pp. 317–331.
doi:10.1243/PIME_PROC_1996_210_204_02